Nanomembrane-Based, Thermal-Transport Biosensor for Living Cells

*Rami T. ElAfandy, Ayman F. AbuElela, Pawan Mishra, Bilal Janjua, Hassan M. Oubei, Ulrich Büttner, Mohammed A. Majid, Tien Khee Ng, Jasmeen S. Merzaban, and Boon S. Ooi**

***K**nowledge of materials' thermal-transport properties, conductivity and diffusivity, is crucial for several applications within areas of biology, material science and engineering. Specifically, a microsized, flexible, biologically integrated thermal transport sensor is beneficial to a plethora of applications, ranging across plants physiological ecology and thermal imaging and treatment of cancerous cells, to thermal dissipation in flexible semiconductors and thermoelectrics. Living cells pose extra challenges, due to their small volumes and irregular curvilinear shapes. Here a novel approach of simultaneously measuring thermal conductivity and diffusivity of different materials and its applicability to single cells is demonstrated. This technique is based on increasing phonon-boundary-scattering rate in nanomembranes, having extremely low flexural rigidities, to induce a considerable spectral dependence of the bandgap-emission over excitation-laser intensity. It is demonstrated that once in contact with organic or inorganic materials, the nanomembranes' emission spectrally shift based on the material's thermal diffusivity and conductivity. This NM-based technique is further applied to differentiate between different types and subtypes of cancer cells, based on their thermal-transport properties. It is anticipated that this novel technique to enable an efficient single-cell thermal targeting, allow better modeling of cellular thermal distribution and enable novel diagnostic techniques based on variations of single-cell thermal-transport properties.*

1. Introduction

Knowledge of the physical properties of living cells, such as electrical, optical, or mechanical has always been an enabler for novel imaging, diagnostic, and therapeutic techniques.[1,2] Dynamic thermal properties and thermal diffusivity, the cell's ability to conduct thermal energy relative to its ability to store it, in particular, play an integral role in understanding how heat energy, whether generated through different biological processes or through artificially inserted heaters, is distributed

R. T. ElAfandy, P. Mishra, B. Janjua, H. M. Oubei, Dr. M. A. Majid, Dr. T. K. Ng, Prof. B. S. Ooi
Photonics Laboratory, Computer, Electrical and Mathematical Sciences and Engineering
King Abdullah University of Science and Technology (KAUST)
Thuwal 23955-6900, Kingdom of Saudi Arabia
E-mail: boon.ooi@kaust.edu.sa

A. F. AbuElela, Prof. J. S. Merzaban
Division of Biological and Environmental Sciences and Engineering
King Abdullah University of Science and Technology (KAUST)
Thuwal 23955-6900, Kingdom of Saudi Arabia

U. Büttner
Microfluidics Core Lab, Computer, Electrical and Mathematical Sciences and Engineering
King Abdullah University of Science and Technology (KAUST)
Thuwal 23955-6900, Kingdom of Saudi Arabia

DOI: 10.1002/smll.201603080

within the cellular environment. A plethora of imaging (photoacoustic[3,4] and photothermal imaging,[5]) diagnostic (cell death monitoring[6]) and therapeutic (photo/magnetothermal cancer targeting[7–9]) techniques, require knowledge of dynamic heat flow within the cells. Other applications, ranging across plants physiological ecology (Xylem sap-flow rates and leaf temperature control),[10,11] to thermal dissipation in flexible semiconductors[12] and flexible thermoelectric generation[13,14] would benefit from a flexible microsized thermal-transport sensor. Living cells, however, due to their relatively small volumes and irregular curvilinear shapes, pose extra challenges in probing their physical-transport properties.[15] Since cellular response to overheating is diverse, ranging from improved diffusion rate across the cellular membrane to irreversible damage and protein denaturation,[16] several techniques were developed to measure cellular thermal-transport properties. 3-Omega[17,18] and thermal lensing[6,19] techniques were employed to measure thermal conductivity and diffusivity (and effusivity as well), respectively. The cellular thermal diffusivity however is not studied as a thermal indicator of different types of cancers or different sub-types of the same cancer.

In this letter, we first study the effect of laser induced heating on the photoluminescence emission spectrum of gallium nitride (GaN) nanomembranes (NMs). We then develop a novel technique to simultaneously measure thermal conductivity and diffusivity of living cells. We base our technique on NMs which, due to their extremely small flexural rigidity,[20] are capable of accommodating the irregular and curvilinear cellular shape for better thermal contact.[21,22] Furthermore, due to their large surface to volume ratio, NMs have been a platform for several bio-detection techniques.[23] We apply our technique to measuring dynamic thermal properties of different living cancer cells. Based on thermal conductivity and diffusivities, we perform multimodal logistic regression to differentiate between different cell lines. We successfully differentiate, for the first time, between different types of cancers (cervical and breast cancers) as well as between subtypes of the same cancer (basal and luminal cancer cells) based on their calculated thermal diffusivities. We also demonstrate that cell lines belonging to the same subgroup have similar (statistically insignificant difference) thermal diffusivities.

The operation principle of our novel technique relies on the ability to spectrally shift the bandgap photoluminescence (PL) emission of GaN NMs through laser-induced heating due to the increased phonons-boundary-scattering rate. As illustrated in **Figure 1**, a pulsed, focused laser beam locally heats an NM that is in direct contact with a living cell. The generated heat energy diffuses to the underlying cell based on its thermal-transport properties. Knowledge of the NM's temperature, obtained by measuring the spectral-shift in its PL emission, yields information of the cell's thermal properties. The function of the gold (Au) microdisc is to block unabsorbed laser radiation to prevent it from being absorbed within the underlying cell as further detailed below. Because GaN is a robust, chemically stable, and biocompatible[24] material we selected GaN NMs in this study. Although fabrication of GaN NMs of different dimensions and crystalline properties has been demonstrated by several groups,[25–28] there is no published work on employing their properties for biomedical applications.

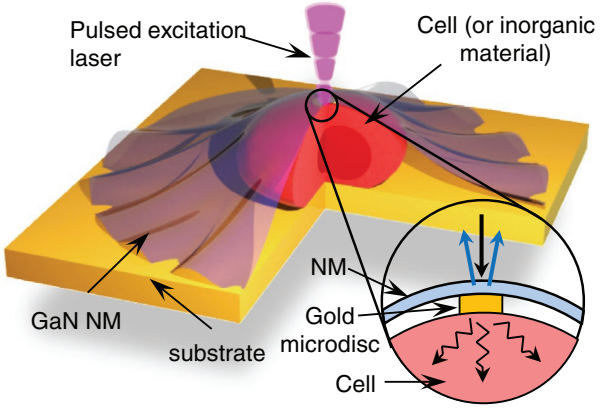

Figure 1. Schematic representation of a cell attached to a substrate and covered with a GaN NM. A pulsed laser beam is focused on the NM to induce local heating as well as PL emission. Because heat spontaneously diffuses from the NM to the cell, the temperature of the NM depends on the cell thermal-transport properties. Consequently, based on the measured temperature-dependent PL emission from the NM, we can estimate the cell thermal-transport properties. The magnified region represents the focused excitation beam (dashed black arrow), which simulates spontaneous bandgap emission (blue arrows) as well as local heat energy which diffuses away from the source (zigzagged black arrows).

2. Results and Discussion

Once excited by a 325 nm (3.81 eV) continuous-wave laser, photo-excited free-excitons emit a series of optical and acoustic phonons while relaxing toward their energy band minimum to conserve energy and momentum simultaneously (**Figure 2**a).[29] Thus, a local nonequilibrium density of phonons (a nonequilibrium temperature gradient) is established, causing the phonons to spontaneously diffuse away from the excitation region into the surrounding crystal. Due to the increase in diffusive phonon-boundary-scattering, the phonon mean free path is reduced to approximately the NM thickness, which causes a reduction in the NM thermal conductivity (κ_{NM}). Therefore, thermal energy is not dissipated rapid enough, and a steady-state increase in local temperature is established, which causes the GaN peak PL emission to redshift with increasing laser excitation intensity.[30]

To measure their PL emission, we transferred the GaN NMs onto a copper grid, and focused a 325 nm laser onto the NMs to a 2.3 μm spot size, as schematically presented in Figure 2b and optically imaged in Figure 2c. The peak PL emissions from 40, 20 and 10 nm thick GaN NMs at increasing laser excitation intensities were measured (Figure 2d). At low-excitation intensity (3.3 μW μm^{-2}), all NMs, regardless of thicknesses, emitted at the same energy (3.42 eV), indicating the absence of laser-induced local heating. However, at increasing excitation intensities, thinner NMs exhibited longer red-shifts as well as wider full width at half maximums (Supporting Information), which is ascribed to an increase in the local temperature due to the increased probability of phonon-boundary-scattering.[31,32]

To calculate κ_{NM} based on the spectral shift, we numerically solved the steady-state heat equation using matrix laboratory (MATLAB) software and then fitted the experimental data. Since the NM thickness is orders of magnitude thinner

DOI: 10.1002/smll.201603080

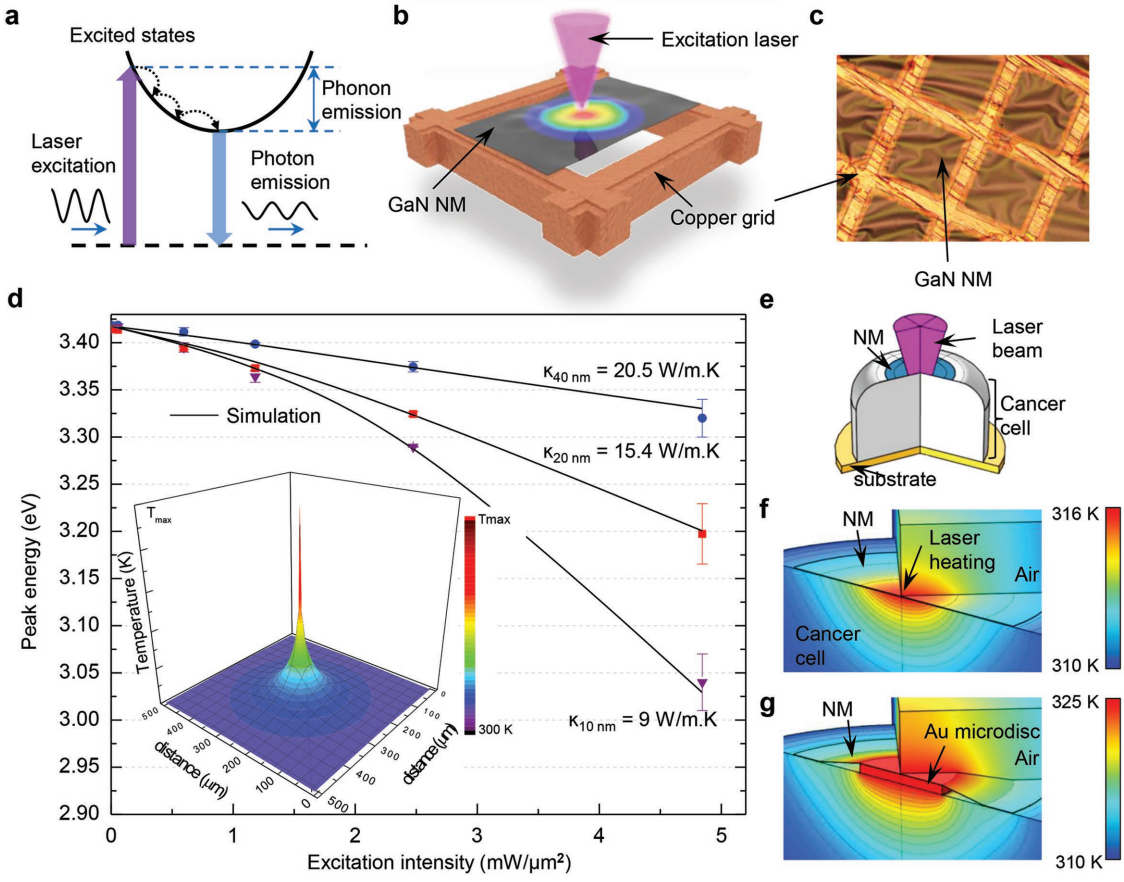

Figure 2. Intensity-dependent PL emissions from NMs. a) Band diagram of the photo-excited free-excitons in GaN showing laser excitation, phonon-assisted relaxation, and PL emission. To measure the laser-induced local heating, we transferred the NMs onto a copper grid as schematically depicted in (b) and optically imaged in (c). d) Experimental and MATLAB simulation results of laser induced heating within NMs of different thicknesses causing an increasing redshift with decreasing NM thickness. Blue circles, red squares, and violet triangles represent the mean measured peak PL emission energy from the 40, 20, and 10 nm thick NMs, respectively. The simulation results are indicated by solid black curves. The Inset plot is the simulated steady-state heat distribution across the NM. e) COMSOL Multiphysics simulation model a laser heated GaN NM attached to a cancer cell with the temperature distribution within the cell when f) the NM is in direct contact and c) when a 250 nm thick, 2.35 μm wide Au microdisc is inserted under the NM.

than its lateral dimensions (40 μm), temperature is assumed constant along its thickness and thus we solved the following 2D heat equation

$$-\kappa_{NM} W_{NM} \nabla^2 T + h_{tot}(T - T_a) + \epsilon\, \sigma_{SB}\left(T^4 - T_a^4\right) = Q_{exc}(x, y) \quad (1)$$

where T and T_a are the NM and ambient temperatures, respectively. h_{tot}, ε, and σ_{SB} are the convection heat transfer coefficient, the GaN emissivity, and the Stefan–Boltzmann constant, respectively. Finally, $Q_{exc}(x, y)$ is the heat power density generated within the NM due to excitation laser, modeled by a Gaussian distribution. The simulated steady-state heat distribution across the NM, plotted in the inset of Figure 2e, indeed showed a steady-state accumulation of heat energy centered on the excitation laser spot. The PL emission energy from the NM was calculated from the local temperature based on Varshni's equation.[33] κ_{NM} of 20.5, 15.4, and 9 W m^{-1} K^{-1} gave the best simulation fit to the experimental data for the 40, 20, and 10 nm thick NMs, respectively (Figure 2d).

In order to simplify our NM based thermal properties measuring technique, a single laser beam is used as "pump" and "probe," simultaneously, with no time gating included at the charge-coupled device (CCD) camera (Detailed experimental setup is in the Supporting Information.) The measured peak PL emission, which represents the integrated PL emissions from the NM during the heating cycle of period τ, is then given by

$$E_{ems}(\tau) = \frac{\int_0^\tau f(T) \times E_{inst}(T)\,dt + \tau \times E_{inst}(RT)}{\int_0^\tau f(T)\,dt + \tau} \quad (2)$$

where $E_{inst}(T)$ and $f(T)$ describe the temporal evolutions in emission peak energy and intensity, respectively; and τ represents the heating period. $E_{inst}(T)$ was calculated after solving the heat diffusion equation within the cell and $f(T)$ was determined experimentally (Further elaboration is in the Supporting Information.) Since Equation (2) contains only two unknowns, namely the cellular thermal conductivity (κ_{cell}) and diffusivity (α_{cell}), they were calculated by pulsing the laser excitation laser beam at two different time periods (τ_1 and τ_2) and then solving the two resulting equations ($E_{ems}(\tau_1)$ and $E_{ems}(\tau_2)$) simultaneously. Furthermore, τ_1 = 100 μs and τ_2 = 7 μs were chosen to be short enough

DOI: 10.1002/smll.201603080

www.MaterialsViews.com

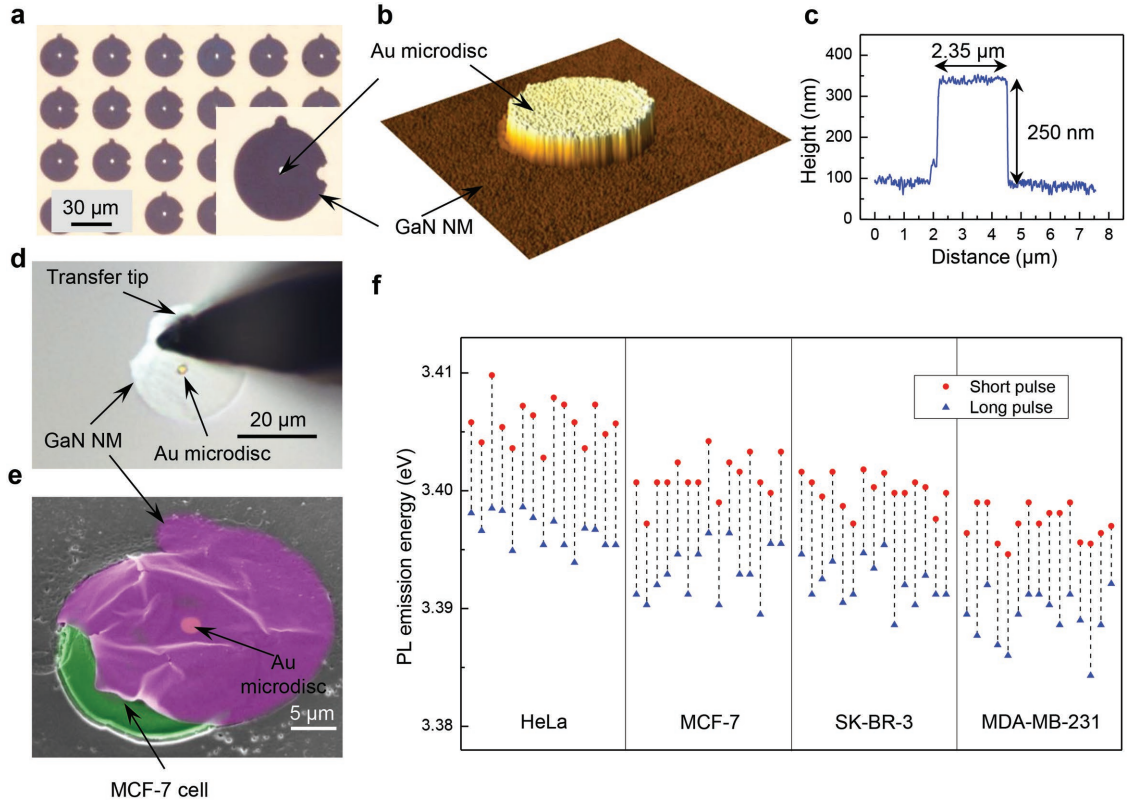

Figure 3. Experimental measurements of thermal-transport properties. a) Optical microscope image of the GaN NMs with the Au microdisc attached while resting on their original GaN substrate. b) AFM image of the Au microdisc, c) with the extracted height profile. d) With a 10 μm wide tungsten tip, we picked individual NMs from the GaN substrate, flipped them, and transferred them to the living cells. e) False-coloured SEM micrograph of a cancer cell (green) covered by a 40 nm thick NM (purple). f) The measured peak PL emission of the NMs attached to two different groups of cancer cell lines (HeLa, MCF-7, SK-BR-3, and MDA-MB-231) due to laser induced heating at different pulse widths.

as to limit heat diffusion to within the cell to prevent any interference from the cell boundary conditions (Supporting Information). COMSOL Multiphysics simulations of the heat diffusion equation within the NM per cell system (Figure 2e) due to a 100 μs long laser pulse are shown in Figure 2f.

Because the NM thickness used in this study (40 nm) was much less than the penetration depth of 325 nm radiation in GaN (≈85 nm), ≈50% of the optical energy was transmitted through the NM. Besides inducing cell damage, this UV transmitted energy would interfere with the measurement due to unwanted heat generation within the underlying cell. To address this issue, we inserted a 250 nm thin Au microdisc under the NM to absorb the transmitted UV energy, while at the same time, due to its high thermal diffusivity (170 $mm^2\ s^{-1}$), does not interfere with the vertical heat diffusion from the NM to the cell (Supporting Information). Furthermore, having a diameter (2.35 μm) close to the laser spot size, the Au microdisc still confines thermal energy which results in a temperature profile similar to the direct contact case (Figure 2g) (Supporting Information).

Through several lithography, metal evaporation and plasma etching techniques, we fabricated 40 μm wide, 40 nm thick GaN NMs with 2.35 μm wide, 250 nm thick Au microdiscs attached to them (optical image in **Figure 3**a, atomic force microscope (AFM) image in Figure 3b and further description in the Experimental Section). With the aid of a 10 μm tungsten tip attached to a micrometer probe positioner, we picked up the NMs (Figure 3d, Video in the Supporting Information), flipped them (so that the Au microdisc is facing down), and transferred them to several materials with different thermal conductivities and diffusivities. We also transferred the NMs to four different cell lines (HeLa cervical cancer, MCF-7, SK-BR-3 ductal breast cancers, and MDA-MB-231 basal breast cancer, Figure 3f, Experimental Section). To eliminate any structural or morphological variations within the NMs and the attached Au microdiscs, which would induce errors within the measurements, we only transferred adjacent NMs from an area of $0.5 \times 0.5\ mm^2$. As observed in Figure 3f, for each cell line, the 100 μs pulse caused a longer PL spectral redshift (blue triangles) than the 7 μs pulse (red circles) due to the increased generated heat energy. More interestingly, each cell line caused a statistically distinct PL spectral shift within the attached NM for the 7 and 100 μs pulses. To prevent the surrounding medium from affecting the detected PL shifts, the cells were taken out from the medium during the measurement. We incubated the adherent cells with trypan blue dye diluted with equal volume of complete culture medium for 2 min to ensure cell viability (Supporting Information).[34]

From the experimentally measured peak PL emission of the NMs attached to different materials (organic or inorganic) we calculated the corresponding thermal conductivity and diffusivity. To evaluate the accuracy of our technique, we calculated the thermal-transport properties of four different materials (**Figure 4**a black circles) and compared the results

DOI: 10.1002/smll.201603080

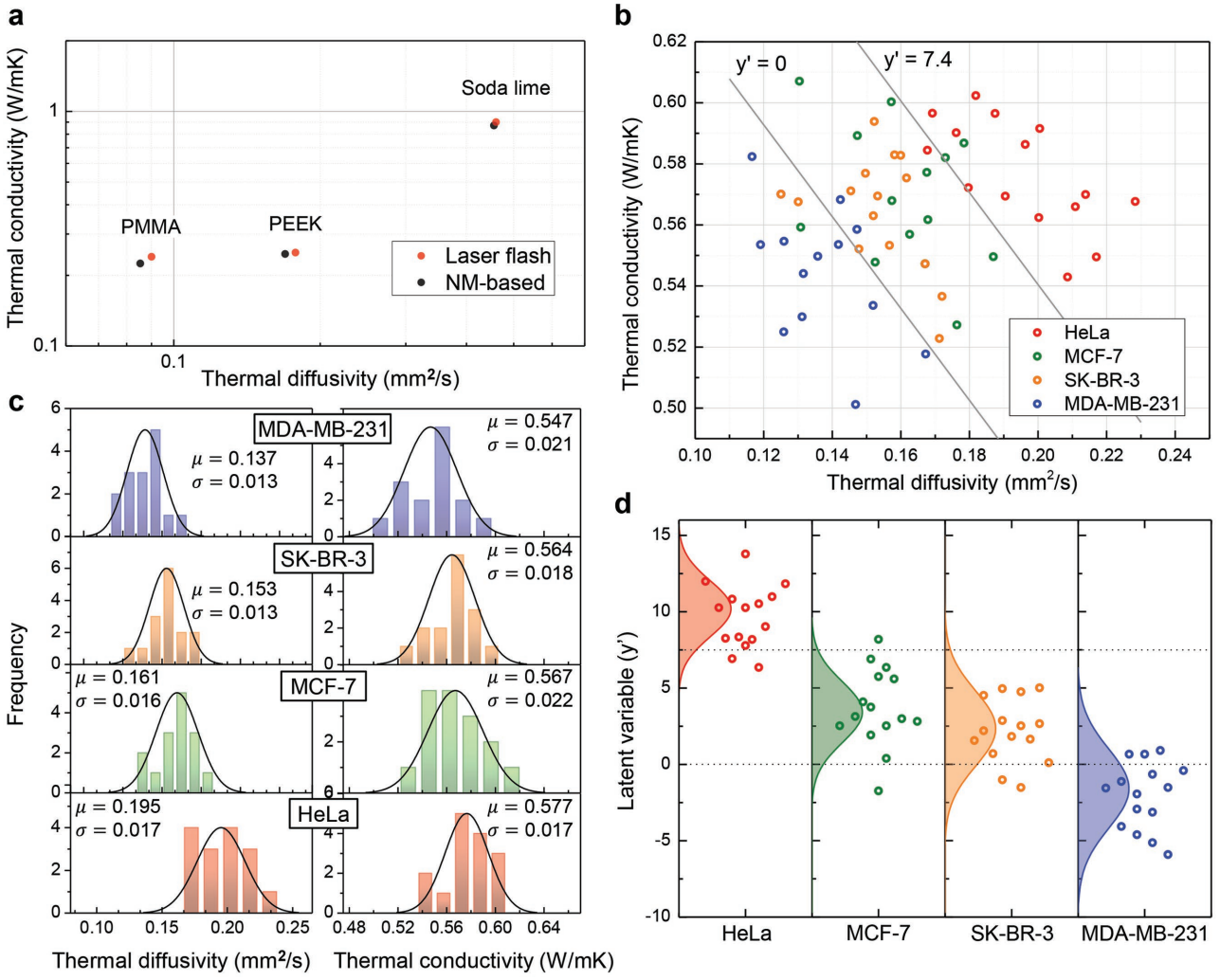

Figure 4. Calculation of thermal-transport properties. a) Thermal conductivity and diffusivity of several materials using the developed NM-based technique (black) and using the laser-flash method (red). b) Scatter diagram of the calculated thermal conductivity and diffusivity of HeLa (red), MCF-7 (green), SK-BR-3 (orange), and MDA-MB-231 (blue) cell lines. The gray curves correspond to the calculated latent variable (y'). Histograms of the calculated values of c) the thermal diffusivity and d) conductivity for the two cell lines with the associated normal distribution fitting (black curves). e) Jitter plot of y', based on the performed multimodal logistic regression, indicating a large difference between cancer cell types as well as between different subtypes.

with the laser flash method (red circles). After calibration, we calculated an average measurement error of 1.7% and 2.7% for conductivity and diffusivity, respectively. After calibration with water, the estimated thermal properties of the four types of cells were then calculated from the peak PL shifts (Figure 3f) and plotted in Figure 4b (60 different cells) with the associated histograms plotted in Figures 4c,d. A one-way analysis of variance (ANOVA) test for the thermal properties of the four different populations showed a statistically significant difference between thermal diffusivity and conductivity means of the four different cell types (p-value (diffusivity) = 2.16×10^{-13} and p-value (conductivity) = 0.002). Based on the different p-values, thermal diffusivity has more predictive power than thermal conductivity. The calculated thermal diffusivity means (μ) for HeLa, MCF-7, SK-BR-7, and MDA-MB-231 were 0.195, 0.161, 0.153, and 0.137 mm^2 s^{-1} (Figure 4c), respectively, and their calculated thermal conductivity means were 0.577, 0.567, 0.564, and 0.547 W mK^{-1}, respectively (Figure 4d). Since the developed technique calculates the thermal conductivity and diffusivity, simultaneously, for the different cell types, we perform a multimodal logistic regression on the acquired data to assess its ability in resolving different cancer cell lines. Applying a latent variable model on the measured data, we reach a latent variable (y') equal to $77.3 - -100\kappa - -150\alpha$ (gray lines in Figure 4b and jitter plot in Figure 4d). Performing an ANOVA test on y', we get a higher degree of separation between the cell lines with a p-value equal to 4.67×10^{-19}. The adjusted p-values, calculated based on Tukey's honest significance test, of the respective pairs are presented in the Supporting Information.

The measured thermal conductivity of the different cell lines were slightly less than that of water ($\kappa = 0.63$ W mK^{-1} at 37 °C), which is consistent with the fact that water normally accounts for ≈80% of the cell's weight.[18] Furthermore, the water content within living cells harbors a large composition

DOI: 10.1002/smll.201603080

of macromolecules, such as proteins, with calculated thermal conductivity less than water,[35,36] thereby contributing to a lower thermal conductivity of living cells.[17] We clearly observe that HeLa (cervical cancer) cells have different y' (and hence thermal properties) from the other breast cancer cell lines demonstrating that thermal properties are different among different types of cancer. Perhaps more interest is that SK-BR-3 and MCF-7, which are both ductal breast cancer cells have statistically different values than MDA-MB-231 luminal breast cancer cells demonstrating the ability of differentiating subtypes (luminal vs basal) of cancer based on their thermal conductivity/diffusivity.

The effect of cellular inner-dynamics, due to different histological origins or different diseases, on the cellular thermal transport is still not properly established.[6] The cellular cytoplasm, due to its both water and protein cytoskeleton (F-actin) contents, is often modeled as a hydrogel.[37] Furthermore, hydrogels, consisting of long polymer chains (similar to the cytoplasm) show an enhancement in their thermal conductivity with an increase in stiffness (characterized by Young's modulus) due to higher polymer density and increased crosslinking.[38,39] Similarly, it is established that cells that have high Young's modulus, also have a high F-actin polymerization density. Interestingly, the published values of Young's moduli of HeLa, MCF-7, and MDA-MB-231 are 2476, 1300, and 750 Pa, respectively.[40,41] Furthermore, SK-BR-3 and MCF-7 are reported to have insignificant differences in their stiffness.[2] We clearly observe the same pattern within the thermal conductivity of the different cell types which suggests thermal transport are correlated with cell stiffness due to the increase in F-actin polymerization. Since cancer cell stiffness is highly correlated to cancer cell invasiveness,[2] the presented data suggests a correlation between cell invasiveness and its thermal properties. We also point out that while there is only a 5% increase in thermal conductivity within the cell types, the thermal diffusivity increased by 42%, indicating that thermal diffusivity serves as a stronger indicator to cancer cell types than conductivity.

In conclusion, we developed a novel thermal conductivity and diffusivity measuring technique based on the transient response of GaN NMs to laser-induced heating. The spatial precision of our technique is controlled by the laser pulse width, which can be varied to increase or decrease the spatial resolution of the object under investigation. We successfully applied our technique in measuring thermal-transport properties of glasses, polymers and living cells. Moreover, we demonstrated that the calculated latent variable y' is useful to differentiate between different types of cancers (cervical and breast) as well as different subtypes of the same cancer (ductal and luminal). Also we observed that cell lines belonging to the same subtype give statistically insignificant differences in their thermal properties (based on the resolution of our technique). Such results lend themselves nicely to numerous biomedical applications, such as high-precision single-cancerous-cell targeting, thermal imaging techniques, detection of cancer types, and assessing cellular health and viability.

3. Experimental Section

NM Fabrication: Using a VEECO GEN930 plasma-assisted molecular beam epitaxy system, a 35 nm thick indium gallium nitride (InGaN) sacrificial layer was grown at 560 °C, followed by 40 nm thick GaN grown at 640 °C, on a 500 nm GaN on a sapphire template wafer. The wafer was then cleaved into 1 cm^2 pieces, which were subsequently degreased in acetone and isopropanol (IPA) for 5 min and then cleaned in nitric acid (HNO_3) at 65 °C for 15 min for surface oxide removal. A thin layer of platinum metal (150 nm) was then deposited near the edge of the top surface. Finally, a layer of AZ resist was spin-coated and patterned into 40 µm wide discs, followed by inductively coupled plasma (ICP) reactive ion etching using an argon (Ar)/chlorine (Cl)-based recipe to expose the InGaN sacrificial layer. The remaining photoresist was then removed with acetone, and the sample was cleaned in IPA.

Au Microdisc Fabrication: A 250 nm thick layer of Au was evaporated onto the sample, followed by a spin-coated layer of SU8-2000.5 photoresist which was then patterned into 2.35 µm discs. Using Ar-bombardment in an ICP reactor, 150 nm of Au was removed, followed by 10 s immersion in potassium iodide (KI)/iodine (I_2) based Au etchant to etch away the remaining 100 nm, leaving behind the intact GaN structure. Finally, oxygen (O_2) plasma was used to remove the remaining SU-8 photoresist.

NM Exfoliation: The samples were immersed in a bath containing CH_3OH: H_2O_2(35%): HF(48%) (1:2:2). Back light illumination was performed by focusing light coming from a 200 W mercury (Hg) arc lamp onto the sample. To selectively etch the InGaN sacrificial layer, any photon energies higher than the GaN bandgap was blocked by placing a polished GaN wafer on top of the etching bath.[42] Once the InGaN was completely etched, the samples were gently cleaned by dipping them in IPA and were then dried using a critical point dryer to enable proper exfoliation of the NM.

PL Measurement: The PL emission from the NM was measured by focusing radiation from a helium–cadmium (He–Cd) gas laser to an average spot of 2.3 µm in diameter. The PL signal was then collected and sent to a 2400 line diffraction grating for dispersion. The authors pulsed the laser by passing the beam through a high-speed chopper. (More details are described in the Supporting Information.)

Cell Culture: Breast cancer cell lines (MCF-7, MDA-MB-231, and SK-BR-3) and the cervical cancer cells line HeLa were purchased from ATCC (Manassas, VA, USA). The MCF-7 cells were cultured in minimum essential medium (MEM) supplemented with 10% foetal bovine serum. 0.01 mg mL^{-1} bovine insulin and penicillin/streptomycin solution (100 units mL^{-1} penicillin, 100 µg mL^{-1} streptomycin) all the other cell lines were cultured in Dulbecco's modified eagle medium (DMEM) supplemented as MEM medium without bovine insulin. All cells were maintained in a humidified incubator at 37 °C and 5% CO_2. In all assays, the cells used were from passages 5 to 25 and were used in suspension or plated on a glass slide (Fisher Scientific Ltd, UK) precoated with attachment factor protein (1X; Fisher Scientific Ltd, UK) for 30 min at 37 °C. All the cells were seeded at a density of $3 \times 10e^5$ cells mL^{-1} (cells cm^{-2}) and incubated at 37 °C and 5% CO_2 in a humidified incubator for 24 h before transferring the NMs onto the cells.

DOI: 10.1002/smll.201603080

Supporting Information

Supporting Information is available from the Wiley Online Library or from the author.

Acknowledgements

R.T.E. conceived, designed, and performed the experiments and numerical simulations and wrote the manuscript. A.F.A. prepared the living cells for measurements and edited the manuscript. P.M. and B.J. performed epitaxial growth of GaN wafers and edited the manuscript. U.B. assisted in experimental setup and approved the manuscript. H.O., M.A.M., T.K.N., and J.S.M. provided useful discussions on the project, discussed the results, and edited the manuscript. B.S.O. supervised the project, discussed the progress and results, and edited the manuscript. The authors acknowledge funding support from King Abdulaziz City for Science and Technology (KACST) Technology Innovation Center (TIC) for Solid State Lighting, grant no. KACST TIC R2-FP- 008, King Abdullah University of Science and Technology (KAUST) baseline funding, grant no. BAS/1/1614-01- 01.

[1] W. H. Grover, A. K. Bryan, M. Diez-Silva, S. Suresh, J. M. Higgins, S. R. Manalis, *Proc. Natl. Acad. Sci. USA* **2011**, *108*, 10992.
[2] Z. Liu, Y. Lee, J. h. Jang, Y. Li, X. Han, K. Yokoi, M. Ferrari, L. Zhou, L. Qin, *Sci. Rep.* **2015**, *5*, 14272.
[3] H. F. Zhang, K. Maslov, G. Stoica, L. V. Wang, *Nat. Biotechnol.* **2006**, *24*, 848.
[4] A. P. Jathoul, J. Laufer, O. Ogunlade, B. Treeby, B. Cox, E. Zhang, P. Johnson, A. R. Pizzey, B. Philip, T. Marafioti, M. F. Lythgoe, R. B. Pedley, M. A. Pule, P. Beard, *Nat. Photonics* **2015**, *9*, 239.
[5] V. P. Zharov, D. O. Lapotko, *IEEE J. Sel. Top. Quantum Electron.* **2005**, *11*, 733.
[6] S. Vasudevan, G. C. K. Chen, M. Andika, *Appl. Phys. Lett.* **2010**, *96*, 113703.
[7] C. Loo, A. Lowery, N. Halas, J. West, R. Drezek, *Nano Lett.* **2005**, *5*, 709.
[8] X. Huang, P. K. Jain, I. H. El-Sayed, M. A. El-Sayed, *Nanomedicine* **2007**, *2*, 681.
[9] M. J. Sailor, J.-H. Park, *Adv. Mater.* **2012**, *24*, 3779.
[10] S. S. O. Burgess, M. A. Adams, N. C. Turner, C. R. Beverly, C. K. Ong, A. A. H. Khan, T. M. Bleby, *Tree Physiol.* **2001**, *21*, 589.
[11] H. Lambers, F. S. Chapin III, T. L. Pxons, *Plant Physiological Ecology*, Springer, New York, USA **2008**.
[12] B. H. Mun, B. K. You, S. R. Yang, H. G. Yoo, J. M. Kim, W. I. Park, Y. Yin, M. Byun, Y. S. Jung, K. J. Lee, *ACS Nano* **2015**, *9*, 4120.
[13] S. W. Finefrock, Y. Wang, J. B. Ferguson, J. V. Ward, H. Fang, J. E. Pfluger, D. S. Dudis, X. Ruan, Y. Wu, *Nano Lett.* **2013**, *13*, 5006.
[14] S. J. Kim, J. H. We, B. J. Cho, *Energy Environ. Sci.* **2014**, *7*, 1959.
[15] V. Kopparthy, N. Crews, presented at *2016 32nd Southern Biomedical Engineering Conference (SBEC)*, March, LA, USA **2016**.
[16] R. W. Y. Habash, R. Bansal, D. Krewski, H. T. Alhafid, *Crit. Rev. Biomed. Eng.* **2006**, *34*, 491.
[17] B. Kyoo Park, N. Yi, J. Park, D. Kim, *Appl. Phys. Lett.* **2013**, *102*, 203702.
[18] B. K. Park, Y. Woo, D. Jeong, J. Park, T.-Y. Choi, D. P. Simmons, J. Ha, D. Kim, *J. Appl. Phys.* **2016**, *119*, 224701.
[19] R. Legrand, M. Abi Ghanem, L. Plawinski, M.-C. Durrieu, B. Audoin, T. Dehoux, *Appl. Phys. Lett.* **2015**, *107*, 263703.
[20] J. Li, J. Zhang, W. Gao, G. Huang, Z. Di, R. Liu, J. Wang, Y. Mei, *Adv. Mater.* **2013**, *25*, 3715.
[21] J. Viventi, D.-H. Kim, J. D. Moss, Y.-S. Kim, J. A. Blanco, N. Annetta, A. Hicks, J. Xiao, Y. Huang, D. J. Callans, J. A. Rogers, B. Litt, *Sci. Transl. Med.* **2010**, *2*, 24ra22.
[22] W. Xi, C. K. Schmidt, S. Sanchez, D. H. Gracias, R. E. Carazo-Salas, S. P. Jackson, O. G. Schmidt, *Nano Lett.* **2014**, *14*, 4197.
[23] C. K. Jeong, H. M. Jin, J.-H. Ahn, T. J. Park, H. G. Yoo, M. Koo, Y.-K. Choi, S. O. Kim, K. J. Lee, *Small* **2014**, *10*, 337.
[24] S. A. Jewett, M. S. Makowski, B. Andrews, M. J. Manfra, A. Ivanisevic, *Acta Biomater.* **2012**, *8*, 728.
[25] R. T. ElAfandy, M. A. Majid, T. K. Ng, L. Zhao, D. Cha, B. S. Ooi, *Adv. Funct. Mater.* **2014**, *24*, 2305.
[26] Y. Mei, D. J. Thurmer, C. Deneke, S. Kiravittaya, Y.-F. Chen, A. Dadgar, F. Bertram, B. Bastek, A. Krost, J. r. Christen, T. Reindl, M. Stoffel, E. Coric, O. G. Schmidt, *ACS Nano* **2009**, *3*, 1663.
[27] I. Tiginyanu, V. Popa, M. A. Stevens-Kalceff, *Mater. Lett.* **2011**, *65*, 360.
[28] S. H. Park, G. Yuan, D. Chen, K. Xiong, J. Song, B. Leung, J. Han, *Nano Lett.* **2014**, *14*, 4293.
[29] D. Kovalev, B. Averboukh, D. Volm, B. K. Meyer, H. Amano, I. Akasaki, *Phys. Rev. B* **1996**, *54*, 2518.
[30] E. Chávez-Ángel, J. S. Reparaz, J. Gomis-Bresco, M. R. Wagner, J. Cuffe, B. Graczykowski, A. Shchepetov, H. Jiang, M. Prunnila, J. Ahopelto, F. Alzina, C. M. Sotomayor Torres, *APL Mater.* **2014**, *2*, 012113.
[31] C. Guthy, C.-Y. Nam, J. E. Fischer, *J. Appl. Phys.* **2008**, *103*, 064319.
[32] S. Piscanec, M. Cantoro, A. C. Ferrari, J. A. Zapien, Y. Lifshitz, S. T. Lee, S. Hofmann, J. Robertson, *Phys. Rev. B* **2003**, *68*, 241312.
[33] N. Nepal, J. Li, M. L. Nakarmi, J. Y. Lin, H. X. Jiang, *Appl. Phys. Lett.* **2005**, *87*, 242104.
[34] W. Strober, *Current Protocols in Immunology*, John Wiley & Sons, Inc., NJ, USA **2001**.
[35] T. J. Müller, F. Müller-Plathe, *Int. J. Quantum Chem.* **2011**, *111*, 1403.
[36] X. Yu, D. M. Leitner, *J. Chem. Phys.* **2005**, *122*, 054902.
[37] J. Fels, S. N. Orlov, R. Grygorczyk, *Biophys. J.* **2009**, *96*, 4276.
[38] T. Zhang, T. Luo, *J. Phys. Chem. B* **2016**, *120*, 803.
[39] J. Zaragoza, N. Babhadiashar, V. O'Brien, A. Chang, M. Blanco, A. Zabalegui, H. Lee, P. Asuri, *PLoS ONE* **2015**, *10*, e0136293.
[40] M.-H. Lee, P.-H. Wu, J. R. Staunton, R. Ros, G. D. Longmore, D. Wirtz, *Biophys. J.* **2012**, *102*, 2731.
[41] T. Kihara, T. Yoshida, S. M. A. Haghparast, J. Miyake, *J. Anal. Sci., Methods Instrum.* **2013**, *3*, 124.
[42] A. R. Stonas, T. Margalith, S. P. DenBaars, L. A. Coldren, E. L. Hu, *Appl. Phys. Lett.* **2001**, *78*, 1945.

Received: September 14, 2016
Revised: September 29, 2016
Published online: